

Comparison of HMG and flat rotation velocities inferred from galaxy-galaxy weak lensing

ROBERT MONJO ^{1,2}

¹*Department of Algebra, Geometry and Topology, Complutense University of Madrid
Pza. Ciencias 3, E-28040 Madrid, Spain, rmonjo@ucm.es*

²*Department of Math and Computer Science, Saint Louis University, Max Aub street, 5, E-28003, Madrid, Spain.*

Submitted to ApJ

ABSTRACT

Despite the success of dark-matter models, unresolved issues require exploring alternatives such as modified gravity theories. In this context, we examine the compatibility of the Hyperconical Modified Gravity (HMG) with galaxy rotation curves inferred from weak-lensing data. The research addresses the existing limitations of Modified Newtonian Dynamics (MOND), which often struggle with universal applicability across different galactic scales. By assuming local validity of General Relativity (GR) and analyzing recent data on circular velocities from galaxy-galaxy weak lensing, our findings interpret the galactic dynamics anomaly as a fictitious acceleration inherited from the cosmic expansion, without invoking dark matter. The results indicate that HMG successfully reproduces flat velocity curves on scales of 1 Mpc slightly better than MOND. Therefore, these observations support HMG as a viable gravitational model, highlighting its potential to account for dynamics on galaxies and other scales. Further research with extensive datasets is required to confirm these preliminary insights.

1. INTRODUCTION

The dark matter paradigm has been remarkably successful in explaining a wide range of astrophysical phenomena, from the rotation curves of galaxies to the large-scale structure of the universe (Clowe et al. 2006; Frenk & White 2012; Bullock & Boylan-Kolchin 2017). However, several open issues persist. Despite extensive efforts, dark matter particles have yet to be detected directly (Roszkowski et al. 2018). Observational anomalies, such as the mass discrepancy-acceleration relation (MDAR) and the baryonic Tully-Fisher relation (BTFR), suggest that our understanding of gravity at galactic scales may be incomplete (McGaugh et al. 2016). In particular, the BTFR is an empirical mass-discrepancy acceleration relation found in galaxy dynamics, which is tightly described as a function of the observed baryonic mass M_b without the need for unobservable matter (Trippe 2014; Merritt 2017; Goddy et al. 2023). This law is commonly expressed as follows:

$$M_b = A v_{\text{flat}}^\epsilon, \quad (1)$$

with $\epsilon \approx 4$ for the level of the *flat* velocity curve v_{flat} observed in a galaxy disk (see for instance Goddy et al. 2023). Similarly, it can be also expressed as a mass-discrepancy acceleration relation (McGaugh 2004; Di Cintio & Lelli 2015),

$$\frac{M_b + M_{\text{CDM}}}{M_b} = \frac{v^2}{v_K^2} = C |a_N|^{-\beta} = C \left(\frac{r}{v_K^2} \right)^\beta \implies v^4 = C^2 r^{2\beta} v_K^{4(1-\beta)} \approx C^2 G M_b \quad (2)$$

where $\beta \approx 0.5$, $M_b + M_{\text{CDM}}$ is the Newtonian dynamical total mass including CDM and $C^2 G \approx: A^{-1}$ is approximately the inverse of the constant used in Eq. 1, and the Newtonian acceleration $|a_N| = GM_b/r = v_N^2/r$ is expressed as a function of the Kepler-Newton velocity v_N and the radial distance r to the galaxy. To explain this phenomena, some studies suggested that dark matter presents a stronger coupling to baryons, linking both matter contents by an effective law (Blanchet 2007; Katz et al. 2016; Barkana 2018). However, most observations suggest the need to modify the standard gravity models because the anomalies only occur where the gravity induced by the visible matter is lower than a typical scale with almost constant value, which points to a more general problem involving scales than a problem involving matter types (Trippe 2014; Merritt 2017; Comerón et al. 2023).

Alternative theories such as the Milgromian Dynamics (MOND), Moffat Gravity (MOG) and Hyperconical Modified Gravity (HMG) propose modifications to gravity that could potentially eliminate the need for dark matter (Milgrom 1983; Moffat & Toth 2009; Milgrom 2020; Monjo 2023).

MOND was introduced by Milgrom in 1983 as an alternative to dark matter. MOND modifies Newton's second law for accelerations below a certain threshold a_0 , leading to the following effective gravitational acceleration:

$$a_{\text{MOND}} = a_N \nu \left(\frac{a_N}{a_0} \right) = \begin{cases} a_N & \text{if } a_N \gg a_0 \\ \sqrt{a_N a_0} & \text{if } a_N \ll a_0 \end{cases}, \quad (3)$$

where $a_0 \approx 1.2 \times 10^{-10} \text{ m/s}^2$ is the characteristic acceleration scale, while $\nu(x)$ is an interpolation function that satisfies $\nu(x) = 1$ for $x \gg 1$ and $\nu(x) = 1/\sqrt{x}$ for $x \ll 1$. The best-fitting ν function is (McGaugh et al. 2016; Banik & Zhao 2022):

$$\nu(x) = \frac{1}{1 - \exp(-\sqrt{x})}. \quad (4)$$

MOND has been successful in explaining the flat rotation curves of spiral galaxies without invoking dark matter (Sanders 2003; McGaugh et al. 2007). However, its extension to a relativistic theory still presents some unsolved challenges, in addition to problems at smaller scales (Banik & Zhao 2022; Monjo 2023; Banik et al. 2024; Cookson 2024).

Hyperconical Modified Gravity (HMG) is a more recent proposal that modifies the gravitational potential by restricting GR to be valid only at a local scale over a background hyperconical metric (Monjo 2024). HMG is a relativistic theory that reproduces the behavior of MOND with a unique natural transition function ν that addresses the shortcomings of MOND in explaining the radial acceleration relation (RAR) of galaxy clusters (Monjo & Banik 2024). Specifically, the HMG transition function depends on the distribution of mass and the geometry of spacetime.

To complete our previous findings, this *letter* analyzes the HMG modeling for flat rotation curves, inferred from weak lensing, recently published (Mistele et al. 2024). To analyze the theoretical circular orbital velocities from weak lensing using a specific Lorentzian metric, the authors widely considered the case of a spherically symmetric metric given by $ds^2 = f(r)c^2 dt^2 - g(r)dr^2 - r^2(d\theta^2 + \sin^2\theta d\phi^2)$, where $f(r)$ and $g(r)$ are functions of the radial coordinate r (Bartelmann & Schneider 2001; Rodríguez-Gil et al. 2005). The enclosed mass $M(r)$ within a radius r is related to the metric functions $f(r)$ and $g(r)$. For a static and spherically symmetric spacetime, $f(r) = g(r)^{-1} = 1 - 2\Phi/c^2$ imitates the Schwarzschild metric, with gravitational potential at r defined by $\Phi(\mathbf{r}) \equiv -G \int \rho(\mathbf{r}')/|\mathbf{r} - \mathbf{r}'| dV'$, where $\rho(r')$ is the mass density at a point r' distributed around the volume V' , and approaches $\Phi(r) = GM(r)/r$ in the classic spherical limit. In the Newtonian regimen, with weak gravity ($r \gg 2GM/c^2$) and low velocities ($v/c \ll 1$), the function $f(r)$ contributes significantly more than the function $g(r)$ to geodesics (Bartelmann & Schneider 2001; Dolan 2023).

As a key in weak lensing analysis, the surface mass density $\Sigma(R)$ at projected distance R is obtained by projecting the mass density $\rho(r)$ along the line of sight according to $\Sigma(R) = 2 \int_0^\infty \rho(\sqrt{R^2 + z^2}) dz$, and the *convergence* or dimensionless surface mass density is given by $\kappa(R) = \Sigma(R)/\Sigma_{\text{crit}}$, where $\Sigma_{\text{crit}} = \frac{c^2}{4\pi G} D_s D_d^{-1} D_{ds}^{-1}$ is the critical surface mass density for lensing, while D_s , D_d , and D_{ds} are the angular diameter distances from the observer to the source, the observer to the lens, and the lens to the source, respectively (see figure 1 of Banik & Zhao 2015). These relationships allow us to derive the mass profile from radial acceleration $a_{\text{obs}}(r)$ and subsequently calculate the theoretical circular orbital (square) velocity $v_c^2(r) := r a_{\text{obs}}(r)$, which is critical for understanding the dynamics of galaxies through weak lensing data (Rodríguez-Gil et al. 2005; Brouwer et al. 2021; Mistele et al. 2024).

2. DATA AND MODEL

2.1. Inferred observations

This *letter* uses the published results of Mistele et al. (2024) on the observed circular velocity inferred from weak lensing and classified in four bins of baryonic mass (1.29, 4.57, 9.13, and 19.5 in units of $10^{10} M_\odot$). Specifically, we use 20 accurate estimates of the *flat* speed (v_{flat}) as a function of the observed mass and distances (table 1 of Mistele et al. 2024). Moreover, our work uses baryonic Tully-Fisher data published in the same paper, distinguishing between ranges of 300 kpc and 1 Mpc, as well as between early-type galaxies (ETGs) and late-type galaxies (LTGs). The results are consistent with Lelli et al. (2019).

2.2. Metric perturbation of HMG

Observed orbital speed data inferred from weak lensing were compared to the values modeled by HMG, for the observed baryonic mass, according to the work developed by [Monjo \(2023\)](#) and [Monjo & Banik \(2024\)](#), which is summarized here. Let g be the background metric of the hyperconical universe ([Monjo 2017](#); [Monjo & Campoamor-Stursberg 2023](#)). The metric g is locally approximately given by

$$g \approx dt^2 (1 - kr'^2) - \frac{t^2}{t_0^2} \left(\frac{dr'^2}{1 - kr'^2} + r'^2 d\Sigma^2 \right) - \frac{2r't}{t_0^2} dr' dt, \quad (5)$$

where $k = 1/t_0^2$ is the spatial curvature for the current value of the age t of the universe ($t_0 \equiv 1$), while t/t_0 is a linear scale factor, $r' \ll t_0$ is the comoving distance, and Σ represents the angular coordinates. The shift and lapse terms of Eq. 5, produced by the comoving observers, lead in turn to an apparent radial spatial inhomogeneity that is assimilated as a fictitious acceleration with adequate projected coordinates.

The HMG model is based on two key ideas:

1. Any gravitational system of mass M_{sys} generates a perturbation over the diagonal terms of the background metric $g \rightarrow \hat{g}$ in Eq. 5, such that $kr'^2 \rightarrow kr'^2 + \int_{r'}^{\infty} 2GM(r)/(c^2 r^2) dr$ with $t \approx t_0$. In other words, GR is only (locally) valid with respect to the background metric ([Monjo 2024](#)), thus gravity dynamics is due to the perturbation term $\hat{h} := \hat{g} - g$,

$$g_{Sch} := \eta + (\hat{g} - g) \approx \left(1 - \int_{r'}^{\infty} \frac{2GM(r)}{c^2 r^2} dr \right) c^2 dt^2 - \left[\left(1 + \int_{r'}^{\infty} \frac{2GM(r)}{c^2 r^2} dr \right) dr'^2 + r'^2 d\Sigma^2 \right]; \quad (6)$$

2. the coordinates that parameterize the metric, are finally projected as follows:

$$\begin{aligned} r' &\rightarrow \hat{r}' = \lambda^{1/2} r' \\ t &\rightarrow \hat{t} = \lambda t \end{aligned}$$

where $\lambda := 1/(1 - \gamma/\gamma_0)$ is the stereographic scaling, which is a function of the angular position $\gamma = \sin^{-1}(r'/t_0)$ and a projection factor $\gamma_0^{-1} = \gamma_{\text{sys}}^{-1} \cos \gamma_{\text{sys}}$, where γ_{sys} is the characteristic angle of the gravitational system. In an empty universe, $\gamma_0 = \gamma_U / \cos \gamma_U$. We expect $\gamma_U = \frac{1}{3}\pi$ and therefore that $\gamma_0 = \frac{2}{3}\pi \approx 2$ ([Monjo & Campoamor-Stursberg 2023](#)).

With these ingredients, minimally-perturbed metric derived by HMG outside a distribution mass is ([Appendix A](#)):

$$\hat{g} \approx \left(1 - \frac{2GM}{c^2 r} + \frac{2r}{\gamma_0(r)ct} \right) c^2 dt^2 - \left[\left(1 + \frac{2GM}{c^2 r} + \frac{2r}{\gamma_0(r)ct} \right) dr^2 + r^2 \left(1 + \frac{r}{\gamma_0(r)ct} \right) d\Sigma^2 \right], \quad (7)$$

where $r/\gamma_0(r)$ approaches to 0 for both $r \rightarrow 0$ and $r \rightarrow \infty$. Alternatively, comoving radial coordinate $r' \equiv (t_0/t) r$ can be used instead of r , but it is assumed to be approximately equivalent for gravitational systems close to the observers.

The spacetime derived from local GR (that is, resulting in Eq. 6) and the one represented by the perturbed metric (Eq. 7) satisfy the requirement to be asymptotically flat and coincide with the diagonal Schwarzschild solution at large distances. Therefore the effective ‘‘enclosed mass’’ can be estimated as usual in weak lensing ([Bartelmann & Schneider 2001](#); [Will 2014](#); [Umetsu 2020](#)). To illustrate the behavior of Eq. 7 for weak gravitational fields, an example of deflection angles is derived in [Appendix B](#).

2.3. Orbital speed and Hubble flux relation

The orbital speed v_C is modeled by HMG according to the geodesic equations obtained for the projected time component of the perturbation \hat{h}_{tt} . As a result, a fictitious cosmic acceleration of $a_{\gamma_0}(r) := \gamma_0(r)^{-1} 2c/t = \gamma_{\text{sys}}^{-1}(r) \cos \gamma_{\text{sys}}(r) 2c/t$ emerges with a non-negligible time-like component, which contributes to the total centrifugal acceleration $a_C(r) = v_C^2/r$ such that ([Appendix A](#)):

$$a_C(r)^2 \approx a_N(r)^2 + |a_N(r)| \frac{2c}{\gamma_0(r)t} \implies \left(\frac{v_C}{v_N} \right)^2 \approx \sqrt{1 + \frac{1}{|a_N|} \frac{2c}{\gamma_0(r)t}}, \quad (8)$$

where $a_N(r) := GM_{\text{sys}}/r^2$ is the Newtonian acceleration and $v_N = \sqrt{a_N(r)r}$ is the circular orbital speed. Notice that Eq. 8 leads to $v_{\text{flat}} = \lim_{r \rightarrow \infty} v_C = [2GM_{\text{sys}}c/(\gamma_0 t)]^{1/4}$ as in Eq. 1. However, assuming that gravitationally-bounded space does not expand (i.e., $r'(t_0) \mapsto r(t) = r'(t_0)$ does not increase) as a function of time $t_0 \mapsto t > t_0$, one could require to use the redshift z for estimating the observed time $t \mapsto t_0 \approx t/(1+z/2)$ in the gravitational system (Monjo 2024).

For modeling observations of circular orbital velocities, the characteristic angle γ_{sys} of the considered system can be estimated from a general approach by considering the relative geometry (angle) between the Hubble speed $v_H(r) := r/t$ and the Newtonian circular speed $v_N(r) := \sqrt{GM_{\text{sys}}/r}$, as follows (Monjo & Banik 2024):

$$\sin^2 \gamma_{\text{sys}}(r) \approx \sin^2 \gamma_U + (\sin^2 \gamma_{\text{center}} - \sin^2 \gamma_U) \left| \frac{2v_N^2(r) - \epsilon_H^2 v_H^2(r)}{2v_N^2(r) + \epsilon_H^2 v_H^2(r)} \right|, \quad (9)$$

where the parameter ϵ_H^2 is the so-called *relative density of the neighborhood*, while $\gamma_{\text{center}} \approx \pi/2$ and $\gamma_U = \pi/3$ can be fixed here to set a 1-parameter (ϵ_H) general model from Eq. 9 instead of fitting an average value γ_0 in the simple γ -HMG version (Eq. 8).

The interpretation of Eq. 9 is the following: The anomaly in galaxy rotation curves is minimal when the projective angle is maximal (i.e., $\gamma_{\text{sys}} = \gamma_{\text{center}}$), reached for the highest velocities $v_N \gg \epsilon_H v_H$ at small radial distances. In contrast, the anomaly is maximum with minimum angle, $\gamma_{\text{sys}} = \gamma_U$, when the Newtonian speed is reduced down to the Hubble flux $v_N = \epsilon_H v_H$ at larger distances (bordering with neighbor systems). Therefore, the model described by Eq. 9 consists of a key parameter ϵ_H that refers to the neighborhood dynamical equilibrium (i.e., $v_N = \epsilon_H v_H$).

In other words, the parameter ϵ_H is not totally free, since it is theoretically and statistically strongly linked to the observed density $\rho(r)$ of the system at $r = r_{\text{nei}} \sim 50 - 200$ kpc, which are neighborhood distances r_{nei} with dynamical equilibrium (Monjo & Banik 2024). In particular, for a typical distance $r_{\text{sys}} < r_{\text{nei}}$, we found that $\frac{1}{6} \leq \epsilon_H^2(r_{\text{sys}}) \leq \frac{1}{6} + \rho(r_{\text{nei}})/\rho_{\text{vac}}$, where $\rho_{\text{vac}} := 3/(8\pi G t^2)$ is the vacuum density. To test its impact on the model, we considered two approaches in this work. On the one hand, we set $\gamma_0(r) = \gamma_0$ as a characteristic constant (at least for each type of system) to simply fit an 1-parameter γ -HMG model (Eq. 8) in a similar way as in the MOND paradigm. On the other hand, we assume an ϵ -HMG version in which $\gamma_0(r) = \gamma_{\text{sys}}(r)/\cos \gamma_{\text{sys}}(r)$ depends on the velocities modulated by ϵ_H^2 as shown in Eq. 9. In turn, ϵ_H is presumed to vary as a function of the system density $\rho(r_{\text{sys}})$ at a given distance r_{sys} , as follows:

$$\epsilon_H^2(r_{\text{sys}}) - \frac{1}{6} \approx \left(\frac{\rho(r_{\text{nei}})}{\rho_{\text{vac}}} \right)^\zeta = \left(\frac{\rho(r_{\text{sys}})}{\rho_{\text{vac}}} \right)^\zeta \left(\frac{r_{\text{sys}}}{r_{\text{nei}}} \right)^{3\zeta}, \quad (10)$$

where $\zeta = 1$ is theoretically derived but a range is empirically found about $0.8 < \zeta \leq 1$ (Monjo & Banik 2024). Therefore, the semi-empirical ϵ -HMG has two parameters, ζ and $r_{\text{nei}}/r_{\text{sys}} \geq 1$, which modulate the equilibrium of the gravitational system (Fig. 1).

Notice that when $\zeta = 1$ and $r = r_{\text{sys}}$ with $\epsilon_H \gg \frac{1}{6}$, the ϵ -HMG model is equivalent to the simplest γ -HMG version, for which the Hubble-Newton dynamical equilibrium ($\gamma_{\text{sys}} = \gamma_U$) is reached at $r = r_{\text{sys}} = r_{\text{nei}}$ in Eq. 9, as it was found for some galaxies in the same study. In contrast, if $\zeta < 1$, the system is not in equilibrium for $r = r_{\text{sys}}$ under the ϵ -HMG approach (Eqs. 9 and 10). Thus, we set $\zeta \approx 0.8$ to estimate $r_{\text{nei}}/r_{\text{sys}}$ for galaxies whose circular orbital speed is clearly higher than the Hubble flux. Finally, flat velocities were modeled by fitting a_0 in MOND and γ_{sys} in γ -HMG, since these constant speeds are independent of radial distances due to their own asymptotic definition (i.e., ϵ -HMG cannot be adequately fitted).

3. RESULTS AND DISCUSSION

The γ -HMG and ϵ -HMG versions of the model and their derived dynamics illustrate the motion of circular orbits in a modified spacetime, reflecting both classical gravitational effects and anomalies due to a distorting acceleration of about $c/(\gamma_0 t) \lesssim 10^{-10} \text{ m/s}^2$. The resulting new terms represent cosmic influences on gravitational phenomena that should be observable in large-scale astrophysical contexts, as our results suggest.

Without considering redshift effects, the best γ -HMG model fitted to *flat* velocities is found for $\gamma_0 = 8.2_{-0.9}^{+1.1}$, which is compatible with the lowest value of $\gamma_0 = 9.8_{-1.3}^{+1.6}$ fitted to circular velocities (Table 1). This fact is not coincidental because γ_0 is not a constant in the HMG paradigm since it decreases for galaxies (Eq. 9) as the radius increases with an almost flat velocity. Similar results are found when the redshift effect is considered: the lowest value of the projection factor for circular velocities ($\gamma_0 = 11.9_{-1.6}^{+1.9}$) is very close to the one obtained for *flat* velocities ($\gamma_0 = 9.8_{-1.1}^{+1.2}$).

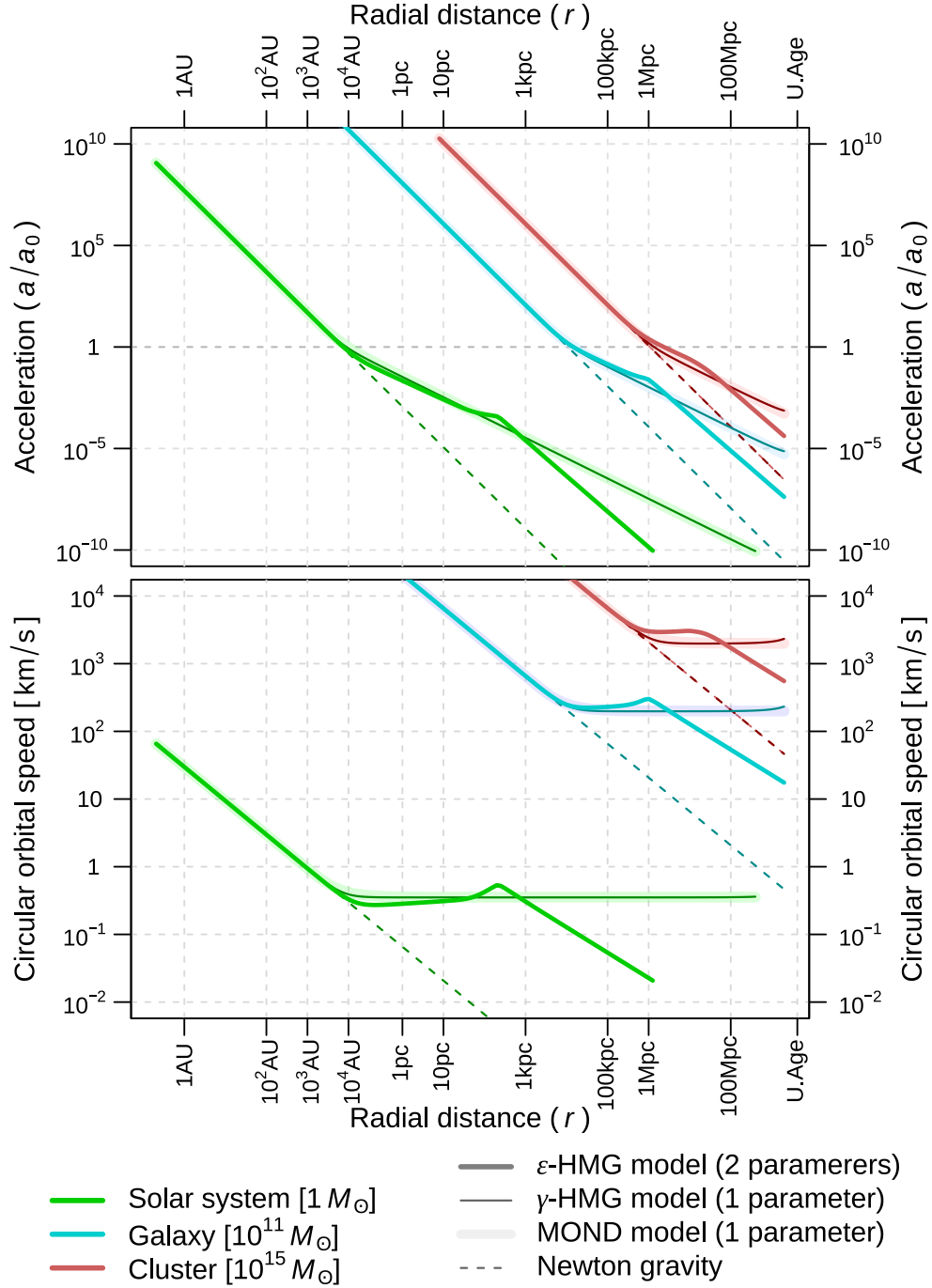


Figure 1. Example of acceleration (top panel) and circular orbital speed (bottom panel) curves, as a function of the radial distance (r), for three gravitational systems centered, respectively, by three characteristic baryonic masses enclosed in r : Sun ($1M_\odot$; green), galaxy ($10^{11}M_\odot$, blue) and galaxy cluster ($10^{15}M_\odot$, red). The models used are: the classical Newtonian gravity (dashed lines), an empirical MOND function (Eq. 4 with standard $a_0 = 1.2 \times 10^{-10} \text{ m/s}^2$; lightly colored width lines), γ -HMG (Eq. 8 with $\gamma_0 = 12$; thin colored lines) and ϵ -HMG (Eqs. 9 and 10 with $r_{\text{sys}} \equiv r$ and different values of $r_{\text{nei}}/r_{\text{sys}}$ and ζ ; width colored lines). The represented ϵ -HMG configurations ($r_{\text{nei}}/r_{\text{sys}}$, ζ) are: (4, 0.9) for the Solar system, (3, 0.9) for the galaxy, and (2, 0.9) for the cluster. The value of $\zeta \equiv 1$ implies that a gravitational system is close to equilibrium with respect to the Hubble flux. The radial distances (r) range between 1 Astronomic Unit (AU) and the maximum *light-travel distance* (t_0c) given by the age t of the Universe (noted as ‘U. Age’, which is $t_0c \approx 13.7 \text{ Gyr } c$ with $c \equiv 1$).

Table 1. Fitting parameters of an empirical MOND interpolation (Eq. 4), γ -HMG (Eq. 8 with $\gamma_0 = \text{constant}$) and ϵ -HMG (Eqs. 9 and 10 with $\zeta = 0.8$) models to observed circular and flat velocities inferred from weak lensing (Mistele et al. 2024). The symbol z is added when redshift is considered via $t_0 \approx t/(1+z/2)$ in the fitting of γ -HMG and ϵ -HMG.

Method	Velocity data	Parameter	χ^2 (p-value)	Best one (*)
MOND	circular	$a_0 = 1.21_{-0.13}^{+0.14} \times 10^{-10} m/s^2$	31.3 (0.96)	-
γ -HMG	circular	$\gamma_0 = 9.8_{-1.3}^{+1.6}$	25.7 (0.86)	-
γ -HMG + z	circular	$\gamma_0 = 11.9_{-1.6}^{+1.9}$	25.9 (0.87)	-
ϵ -HMG	circular	$r_{\text{nei}}/r_{\text{sys}} = 2.5_{-0.4}^{+0.5}$	18.0 (0.48)	-
ϵ -HMG + z	circular	$r_{\text{nei}}/r_{\text{sys}} = 2.9_{-0.5}^{+0.7}$	17.5 (0.44)	*
MOND	flat	$a_0 = 1.63_{-0.20}^{+0.23} \times 10^{-10} m/s^2$	26.1 (0.38)	-
γ -HMG	flat	$\gamma_0 = 8.2_{-0.9}^{+1.1}$	24.5 (0.30)	*
γ -HMG + z	flat	$\gamma_0 = 9.8_{-1.1}^{+1.2}$	25.0 (0.32)	-

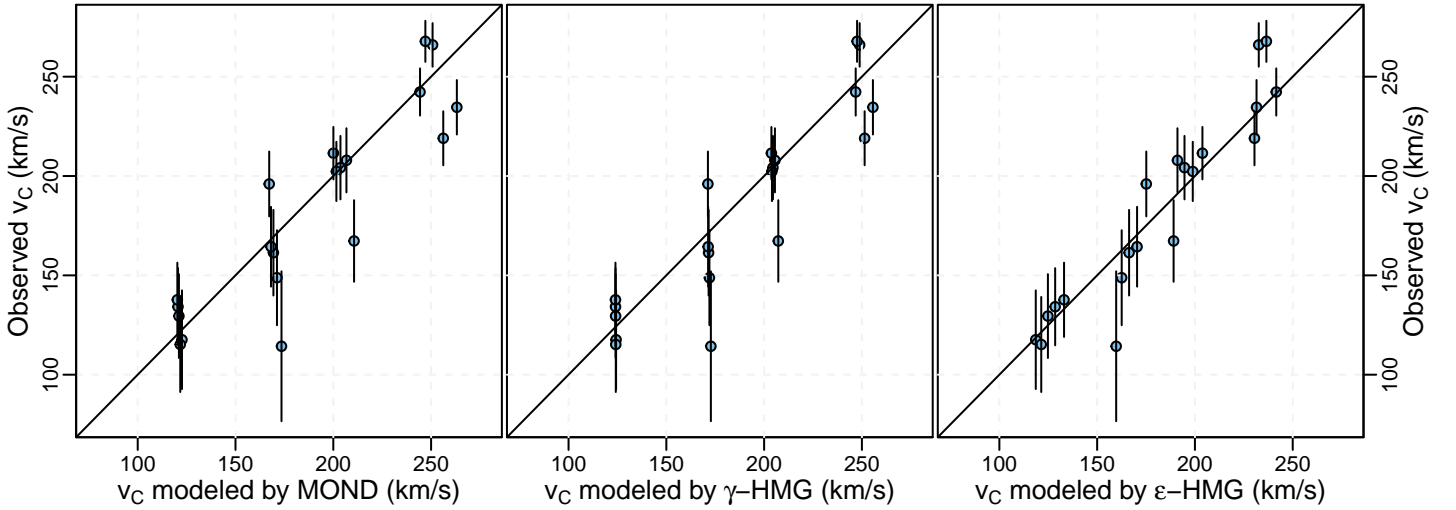


Figure 2. Modeling of circular speed assuming the current time $t \approx t_0$ (i.e., no redshift effects) according to an empirical MOND function (Eq. 4 with $a_0 = 1.21 \times 10^{-10} m/s^2$; left panel), γ -HMG (Eq. 8 with $\gamma_0 = 9.8$; medium panel) and ϵ -HMG (Eqs. 9 and 10 with $\zeta = 0.8$ and $r_{\text{nei}}/r_{\text{sys}} = 2.5$; right panel). These models are fitted to the observed circular velocity inferred from weak lensing (Table 1 of Mistele et al. 2024). Data are gathered in four sets according to four baryonic mass bins (1.29, 4.57, 9.13, and 19.5 in units of $10^{10} M_\odot$).

On the other hand, the MOND parameter $a_0 = 1.21_{-0.13}^{+0.14} \times 10^{-10} m/s^2$ fitted to circular velocities is incompatible with the *flat* velocities analyzed in this work (Fig. 3), and is 3σ -separated with respect to the best fit ($a_0 = 1.63_{-0.20}^{+0.23} \times 10^{-10} m/s^2$). This MOND-based best fit presents a poor result (χ^2 p-value > 0.95) in 2σ -tension with respect to the standard value of $a_0 = 1.2 \times 10^{-10} m/s^2$, which is assumed to be a universal constant. Moreover, the fitting of the ϵ -HMG model showed qualitatively better results in explaining the circular velocities self-consistently compared to the MOND and γ -HMG models (Fig. 2).

The impact of the redshift on the above findings is not statistically significant for modeling observations of circular orbital velocities (Table 1 and Fig. 2). The explanation is that gravity strongly binds its spatial coordinates, mostly removing the effect of expansion, so $r = r'$. In contrast, the flat velocity v_{flat} approaches the external limit of the gravitational force, and therefore the Hubble law $r'/t_0 \approx r/t$ is approximately satisfied. From this effect, the observed cosmic acceleration is practically invariant under the observable time periods (i.e., the dependence on redshift is weak). This finding is consistent with emergent data on the rotation curves of disk galaxies at significant redshifts (Bekenstein & Sagi 2008; McGaugh et al. 2016).

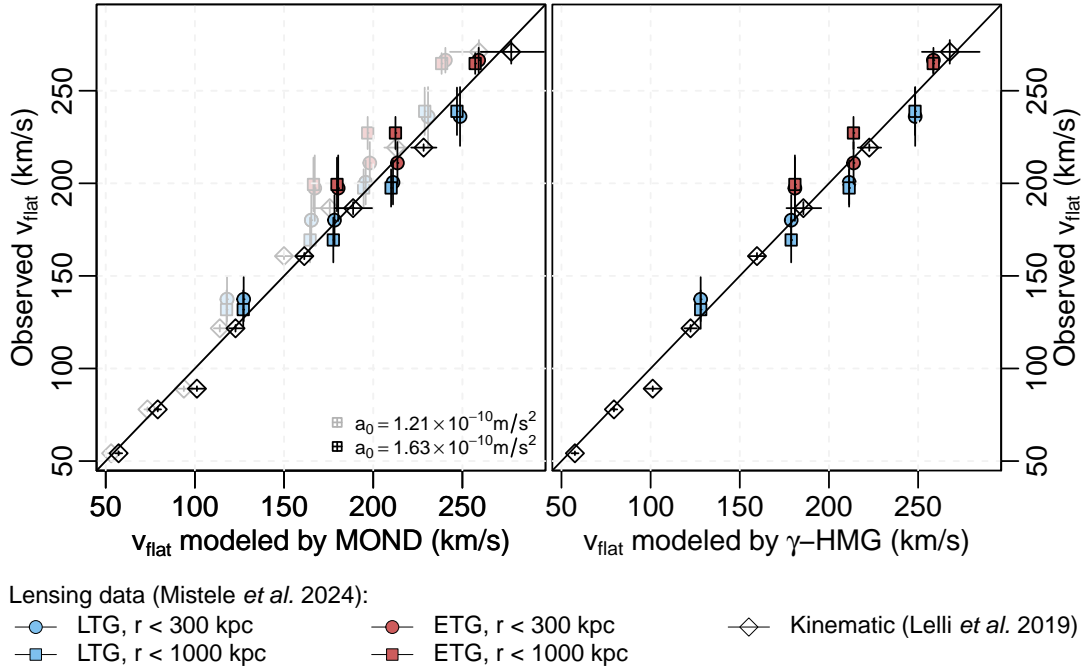


Figure 3. Flat velocity (asymptotic speed of the rotation curve) according to weak lensing observations for ETGs and LTGs separately (red and blue symbols; Mistele *et al.* 2024) and kinetic data (white diamonds; Lelli *et al.* 2019). The left panel shows values from the empirical MOND function with $a_0 = 1.21 \times 10^{-10} \text{m/s}^2$ (light colors), fitted with circular speeds (Table 1) and with $a_0 = 1.63 \times 10^{-10} \text{m/s}^2$ (dark colors) fitted to flat velocities. The right panel shows the γ -HMG model fit to flat velocities with $\gamma_0 = 8.2$.

4. CONCLUDING REMARKS

According to the HMG model, the Newtonian gravitational acceleration is modified by a distorting term $c/(\gamma_0 t)$ that represents a fictitious acceleration inherited from the large-scale effects of comoving reference frames. The modified gravity results in an additional multiscale cosmic acceleration offset but with a special print on galactic dynamics.

The analysis of circular velocities inferred from weak lensing observations suggests the viability of HMG as an alternative to the *dark matter* paradigm, providing a relativistic cosmic approach to the MOND regime. By fitting the observed data to the model, we demonstrate that HMG can reproduce the flat velocity curves even for the 1 Mpc scale, without requiring unobservable particles. Our findings showed that the circular and flat rotation curves are statistically independent of the redshift, which suggests that the coupling of the cosmic acceleration to the perturbed metric in the local GR is very weak. However, the wide-scale flexibility of fitting and the cosmological basis of HMG provide a consistent and potentially more fundamental explanation for the observed gravitational phenomena in galaxies. Although our preliminary findings reinforce the viability of the theory, future studies with larger datasets and more refined versions are needed to validate these results and explore the full implications of HMG on our understanding of cosmology and gravity. Complementary work is now being carried out aligned with reproducing the cosmic microwave background spectrum and the Big Bang nucleosynthesis using the timeline simulated by Monjo & Campoamor-Stursberg (2023).

ACKNOWLEDGEMENTS

The authors thank T. Mistele for providing all the necessary data for this study, as well as for all comments and suggestions. We also acknowledge the contributions of our colleague I. Banik for the valuable feedback and discussions, especially on the interpretation of multiscale behavior of the HMG model.

DATA AVAILABILITY

In this study, no new data was created or measured.

APPENDIX

A. MINIMALLY PERTURBED METRIC AND CIRCULAR ORBITAL VELOCITY

This appendix derives the low acceleration limit from the weak-perturbed field given by the hyperconical model and examines the geodesic equations. Let g be a first-order metric obtained from local GR assuming an approximately unitary scale factor ($t/t_0 \approx 1$) for gravitational systems with mass $M(r')$ enclosed in the radial coordinate r' (Monjo 2024):

$$g \approx \left(1 - \int_{r'}^{\infty} \frac{2GM(r)}{c^2 r^2} dr\right) dt^2 - \left(1 + \int_{r'}^{\infty} \frac{2GM(r)}{c^2 r^2} dr\right) dr'^2 - r'^2 d\Sigma^2, \quad (\text{A.1})$$

where Σ represents the angular coordinates with $d\Sigma = \sin\theta d\theta d\phi$. For instance, consider the most simple case with perturbation compatible with the 1/2-distorting stereographic projection of Monjo & Campoamor-Stursberg (2023), which is obtained from the following differential transformations assuming an almost constant $\gamma_0 = \gamma_0(r') \geq 2$:

$$r' \rightarrow \hat{r}' \approx \left(1 + \frac{r'}{2\gamma_0(r')ct_0}\right) r' \quad \Rightarrow \quad dr' \rightarrow d\hat{r}' \approx \left(1 + \frac{r'}{\gamma_0(r')ct_0}\right) dr' \quad (\text{A.2})$$

$$t \rightarrow \hat{t} \approx \left(1 + \frac{r'}{\gamma_0(r')ct_0}\right) t \quad \Rightarrow \quad dt \rightarrow d\hat{t} \approx \left(1 + \frac{r'}{\gamma_0(r')ct_0}\right) dt + \text{neglected terms} \quad (\text{A.3})$$

Substituting these transformations into the metric $g = g_{ij}dx^i dx^j$, the resulting minimally-perturbed metric \hat{g} is:

$$\hat{g} \approx \left(1 - \int_{r'}^{\infty} \frac{2GM(r)}{c^2 r^2} dr + \frac{2r'}{\gamma_0 ct_0}\right) c^2 d\hat{t}^2 - \left[\left(1 + \int_{r'}^{\infty} \frac{2GM(r)}{c^2 r^2} dr + \frac{2r'}{\gamma_0 ct_0}\right) d\hat{r}'^2 + r'^2 \left(1 + \frac{r'}{\gamma_0 ct_0}\right) d\Sigma^2\right]. \quad (\text{A.4})$$

To analyse cosmic effects, we define an expanding coordinate $r \equiv (t/t_0)r'$, which is practically indistinguishable from the comoving coordinate r' for gravitational systems, but it is a key for large scales. Therefore, the approaches $\frac{2GM}{c^2 r'} \approx \frac{2GM}{c^2 r} \ll 1$ and $\frac{2r'}{\gamma_0 ct_0} \approx \frac{2r}{\gamma_0 ct} \ll 1$ are assumed for the weak-field limit.

According to GR, the geodesic equations are expressed as $\ddot{x}^\mu + \Gamma_{\nu\sigma}^\mu \dot{x}^\nu \dot{x}^\sigma = 0$, where $\Gamma_{\nu\sigma}^\mu \equiv \frac{1}{2}g^{\mu\lambda}(\partial_\sigma g_{\lambda\nu} + \partial_\nu g_{\lambda\sigma} - \partial_\lambda g_{\nu\sigma})$ are the Christoffel symbols and $\dot{x}^\mu \equiv dx^\mu/d\tau$ is the derivative by the proper time τ . The geodesic equations can also be derived from the Lagrangian $\mathcal{L} = (g_{\mu\nu}\dot{x}^\mu \dot{x}^\nu)^{1/2}$ that provide the Euler-Lagrange equations $\frac{d}{d\tau}(\partial\mathcal{L}/\partial\dot{x}^\mu) - \partial\mathcal{L}/\partial x^\mu = 0$. From this approach, a classical-like conservation of the energy E is easily found as follows:

$$E \approx \left(1 - \int_r^{\infty} \frac{GM(r')}{c^2 r'^2} dr' + \frac{r}{\gamma_0 ct} - \frac{1}{2} \frac{\nu^2}{c^2}\right) m_0 c^2. \quad (\text{A.5})$$

where m_0 is the mass of a test particle and ν is its speed. Since secondary terms of $c dt/d\tau \approx 1 + GM/(c^2 r) - r/(\gamma_0 ct) \approx 1$ only contribute to negligible terms in the geodesic equations, total acceleration of a test particle placed at the position $s = te_t + re_r$ with respect to a mostly central mass M is

$$a_s \equiv \frac{d^2 s}{c^2 dt^2} \approx \frac{d^2 s}{d\tau^2} \approx -\frac{r}{\gamma_0 ct^2} e_t - \left(\frac{GM}{c^2 r} + \frac{1}{\gamma_0 ct}\right) e_r. \quad (\text{A.6})$$

Interpretation of Eq. A.6 is that centrifugal acceleration should also have both time-like and space-like components. Specifically, time-like component of the acceleration measured by an observer living in the hyperconical universe is expected to be proportional to $1/(ct)$ as the spatial contribution is proportional to $1/r$. Therefore, total centrifugal acceleration should be

$$a_s = \frac{d^2 s}{c^2 dt^2} = -\frac{\omega_t^2}{c^2} ct e_t - \frac{\omega_r^2}{c^2} r e_r = -\frac{1}{ct} \frac{v_t^2}{c^2} e_t - \frac{1}{r} \frac{v_r^2}{c^2} e_r \quad (\text{A.7})$$

where $\omega_t^2 \equiv v_t^2/(ct)^2$ and $\omega_r^2 \equiv v_r^2/r^2$ are the squared angular speeds in the time- and space-like directions, respectively, while v_t^2 and v_r^2 are tangential squared speeds. Finally, we **hypothesize** that observers measure an effective centrifugal acceleration given by an apparent circular orbital speed v around a radial distance τ , such as:

$$\|a_s\| = \frac{1}{\tau} \frac{v^2}{c^2} = -\frac{1}{\tau} \left\| \frac{v_t^2}{c^2} e_t + \frac{v_r^2}{c^2} e_r \right\| \quad (\text{A.8})$$

Thus, taking into account the Eqs. A.6 and A.7, the absolute value of the speed v is given by

$$\frac{v^4}{c^4} = - \left\| \frac{v_t^2}{c^2} e_t + \frac{v_r^2}{c^2} e_{\bar{r}} \right\|^2 \approx - \left[\left(\frac{r}{\gamma_0 c t} \right)^2 - \left(\frac{GM}{c^2 r} + \frac{r}{\gamma_0 c t} \right)^2 \right] \approx \left(\frac{GM}{rc^2} \right)^2 + \frac{2GM}{\gamma_0 t c^3},$$

which satisfies two well-known limits of Newton's dynamics and the Milgrom's MOND:

$$v \approx \sqrt{\frac{GM}{r}} \quad \text{if } a_N(r) \gg \frac{2c}{\gamma_0 t} \simeq a_0 \quad (\text{A.9})$$

$$v \approx \sqrt[4]{\frac{2GMc}{\gamma_0 t}} \quad \text{if } a_N(r) \ll \frac{2c}{\gamma_0 t} \simeq a_0, \quad (\text{A.10})$$

where $a_N(r) \equiv GM/r^2$ is the classical Newtonian acceleration, a_0 is the Milgrom's constant acceleration and $M = M(r)$ is the total mass within the central sphere of radius r . Notice that the velocity curve $v = v(r)$ can be reworded in terms of the Kepler-Newton speed $v_N(r) := \sqrt{GM(r)/r}$ leading to a mass-discrepancy acceleration relation:

$$v^4 = v_N^4 + v_N^2 r \frac{2c}{\gamma_0 t} \implies \frac{M_{\text{eff}}(r)}{M(r)} = \frac{v^2(r)}{v_N^2(r)} = \sqrt{1 + \frac{1}{|a_N(r)|} \frac{2c}{\gamma_0 t}}, \quad (\text{A.11})$$

with $M = r v_N^2/G$ is the baryonic mass and $M_{\text{eff}} = r v^2/G$ is the apparent total or effective mass.

B. DEFLECTION ANGLE IN HMG

This appendix summarizes the method of Gibbons & Werner (2008) based on the Gauss-Bonnet theorem to derive the deflection angle ($\hat{\varphi}$) by integrating the Gaussian curvature (K) over a domain exterior to the lens, thus providing a geometrically insightful perspective on gravitational lensing by using its related optical metric. The Gauss-Bonnet theorem describes the geometry of a surface D in relation to its topology, which is given by

$$\iint_D K dA + \oint_{\partial D} \kappa_g ds + \sum_i \theta_i = 2\pi\chi(D) \implies \text{Weak lensing: } \hat{\varphi} \equiv \sum_i \theta_i = - \iint_{D_2} K dA, \quad (\text{B.1})$$

where k_g is the geodesic curvature, α_i are the exterior angles and $\chi(D)$ is the Euler characteristic for a domain D . For weak gravitational lensing, the Gaussian curvature K is related to the gravitational potential around the lensing mass. The geodesic curvature k_g is typically zero along the asymptotically flat boundary at infinity, contributing negligibly to the theorem. The exterior angles α_i account for the deficit angles due to spacetime curvature, directly relating to the light deflection angle $\hat{\varphi}$, where $\sum_i \alpha_i = -\varphi$. The Euler characteristic $\chi(D)$ of the exterior domain is zero because the domain is non-compact and asymptotically resembles a flat plane with holes. By integrating the Gaussian curvature and accounting for the exterior angles, Gibbons and Werner's method effectively captures how light bends around a gravitational lens, providing a straightforward and intuitive framework for calculating lensing effects in weak gravitational fields (Li & Zhou 2020).

In our case, let $g = g_{tt}dt^2 + g_{rr}dr^2$ be the metric defined by Eq. A.4. Both the g_{tt} and g_{rr} components contribute to the deflection angle of light. However, the time dilation represented by g_{tt} plays a dominant role in determining the amount of bending that occurs, particularly because it directly represents the gravitational influence on the energy of photons. Finally, the interaction between the time dilation and spatial curvature effects (via the optical metric σ) leads to the observable phenomenon of gravitational lensing. Therefore, in weak-field approximations, where $2GM/c^2 \ll 1$, the Newtonian-like potential (from g_{tt}) gives the leading contribution to light bending, consistent with the classical expectation that gravity acts like a potential well that bending paths in its vicinity. Specifically, the optical metric σ related to g is defined by the null geodesics ($ds^2 = g'_{ij}dx^i dx^j = 0$), and simplifying for the equatorial plane ($\theta = \pi/2$) for outside the mass distribution, it is:

$$\sigma = \frac{g_{rr}}{g_{tt}} dr^2 + \frac{g_{\phi\phi}}{g_{tt}} d\phi^2 \approx \left(1 + \frac{4GM}{c^2 r} \right) dr^2 + r^2 \left(1 + \frac{2GM}{c^2 r} - \frac{r}{\gamma_0(r) c t(r)} \right) d\phi^2, \quad (\text{B.2})$$

where Maclaurin expansion was used for the smallest terms and $t(r) = t_0 - r/c$ is considered to model effects from the early epochs of the Universe. Assuming that $\partial_r \gamma_0(r) \ll \gamma_0(r)/r$, the Gaussian curvature K is dominated by the

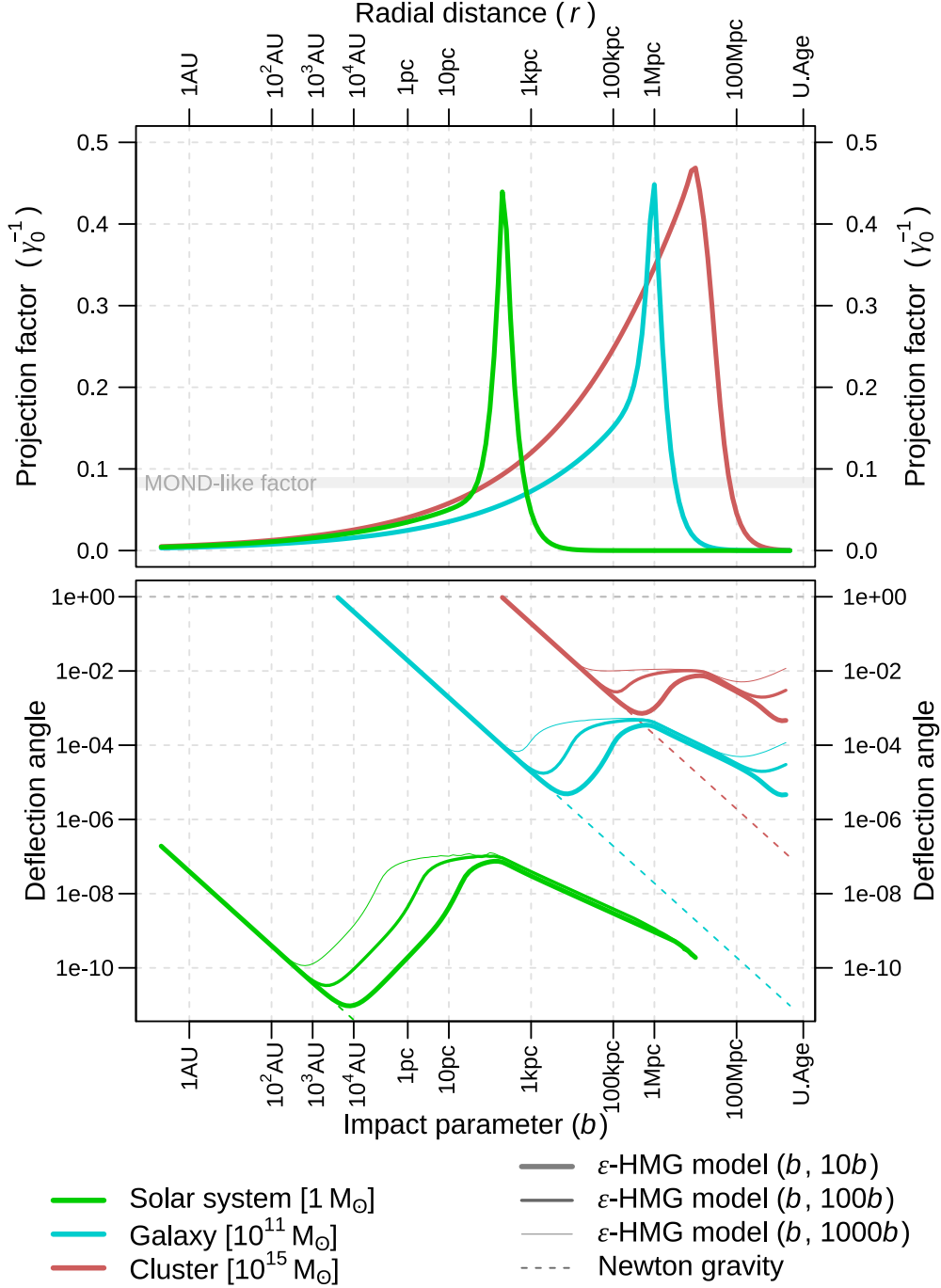


Figure B.1. Example of projection factor (top panel) and corresponding deflection angle in radians (bottom panel) as a function of the impact factor (b) equal to the radial distance (r), for three gravitational systems centered, respectively, by three characteristic baryonic masses enclosed in r : Sun ($1M_\odot$; green), galaxy ($10^{11}M_\odot$, blue) and galaxy cluster ($10^{15}M_\odot$, red). The models used are: the classical Newtonian gravity (dashed lines), and ϵ -HMG (Eqs. 9 and 10 with $r_{\text{sys}} \equiv r$ and different values of $r_{\text{nei}}/r_{\text{sys}}$ and ζ ; width colored lines). The represented ϵ -HMG configurations ($r_{\text{nei}}/r_{\text{sys}}, \zeta$) are: (4, 0.9) for the Solar system, (3, 0.9) for the galaxy, and (2, 0.9) for the cluster. In the top panel, a MOND-like factor of $\gamma_0^{-1} \approx 1/12$ is shown in a thick gray band to represent the Milgromian constant $a_0 \approx 2\gamma_0^{-1}c/t \approx 1.2 \times 10^{-10} \text{ m/s}^2$. The radial distances (r) range between 1 Astronomic Unit (AU) and the maximum *light-travel distance* (t_0c) given by the age t estimated for the Universe (noted as ‘U. Age’, which is $t_0c \approx 13.7 \text{ Gyr } c$ with $c \equiv 1$). To solve the integral of Eq. B.4 in the bottom panel, the age of the Universe was considered with delay (i.e., $t \equiv t_0 - r/c$) and the domain of the radial distance (r) was ranged from b to three different maximum values: $10 \times b$ (thickest colored lines), $10^2 \times b$ (intermediate colored lines) and $10^3 \times b$ (thinnest colored lines).

crossing derivatives of (r, ϕ) over the component $\sigma_{\phi\phi} = g_{\phi\phi}/g_{tt}$ that are given by the Riemann tensor $R_{r'\theta r'\theta}$ of the optical metric σ , that is,

$$K = -\frac{R_{r'\theta r'\theta}}{\det \sigma} \approx \frac{2GM}{c^2 r^3} + \frac{1}{\gamma_0(r) r c t(r)}, \quad (\text{B.3})$$

where $\gamma_0(r) = \gamma_{\text{sys}}(r)/\cos \gamma_{\text{sys}}(r)$ and $\det \sigma = \sigma_{rr}\sigma_{\phi\phi} \approx 1$ is the determinant of the optical metric. The vacuum value of the projective factor is approximately $\gamma_0(r) \approx 2$ (Monjo & Campoamor-Stursberg 2023).

Since the area element is $dA = \sqrt{g_{rr}g_{\phi\phi}} dr d\phi \approx r dr d\phi$, and integrating from $b/\sin(\phi)$ to the source of light (s.l), the deflection angle outside the mass distribution is:

$$\hat{\phi} = \int_{\delta}^{\pi-\delta} \int_{b/\sin(\phi)}^{\text{s.l.}} \left(\frac{2GM}{c^2 r^3} + \frac{1}{\gamma_0(r) r c t(r)} \right) r dr d\phi \approx \frac{4GM}{c^2 b} + \int_{\delta}^{\pi-\delta} \int_{b/\sin(\phi)}^{\text{s.l.}} \frac{\cos \gamma_{\text{sys}}(r)}{c t(r) \gamma_{\text{sys}}(r)} dr d\phi, \quad (\text{B.4})$$

with $0 < \delta \ll 1$ and $t(r) = t_0 - r/c$. Considering Eq. 9, the contribution of the second part can be integrated by using standard numerical techniques (e.g., Simpson's rule), and it is shown in Fig. B.1.

For instance, the deflection angle for a typical galaxy ($M = 10^{11} M_{\odot}$ of baryonic mass) and impact parameter $b = 10 \text{ kpc}$ is $\hat{\phi}_{\text{GR}} \approx 10^{-5}$ rad according to GR. However, the contribution of HMG is $\hat{\phi}_{\text{HMG}} > 10^{-4}$ rad, which could be assimilated as dark-matter phenomenology at these distances. For the Sun ($M_{\odot} = 1.989 \times 10^{30} \text{ kg}$) with an impact parameter of about $b = R_{\odot} = 6.96 \times 10^8 \text{ m}$, the deflection angle is about $\hat{\phi}_{\text{Sun}} \approx 1.75 \text{ arcsec} \approx 8.5 \times 10^{-6}$ rad, and 3.9×10^{-8} rad for $b = 1 \text{ AU}$. The cosmic contribution to the deflection angle predicted by the hyperconical model is about 10^{-15} rad for these short distances, and it is only significant from the radius of 10^3 AU and extends effects beyond to $10^5 \text{ AU} \sim 0.5 \text{ pc}$, which corresponds approximately to the hypothetical Oort Cloud extension (Crovisier 2011). Nevertheless, the predicted deflection angle for the outer solar system seems to be too large since it is extrapolated from the ϵ -HMG parameters fitted with galaxies and clusters. Therefore, a specific analysis is required in future work.

REFERENCES

- Banik, I., Pittordis, C., Sutherland, W., et al. 2024, *MNRAS*, 527, 4573
- Banik, I., & Zhao, H. 2015, *Monthly Notices of the Royal Astronomical Society*, 450, 3155. <https://doi.org/10.1093/mnras/stv802>
- . 2022, *Symmetry*, 14, doi:10.3390/sym14071331. <https://www.mdpi.com/2073-8994/14/7/1331>
- Barkana, R. 2018, *Nature*, 555, 71. <https://doi.org/10.1038/nature25791>
- Bartelmann, M., & Schneider, P. 2001, *Physics Reports*, 340, 291. <https://www.sciencedirect.com/science/article/pii/S037015730000082X>
- Bekenstein, J. D., & Sagi, E. 2008, *Phys. Rev. D*, 77, 103512. <https://link.aps.org/doi/10.1103/PhysRevD.77.103512>
- Blanchet, L. 2007, *CQGra*, 24, 3529. <https://dx.doi.org/10.1088/0264-9381/24/14/001>
- Brouwer, M. M., Oman, Kyle A., Valentijn, Edwin A., et al. 2021, *A&A*, 650, A113. <https://doi.org/10.1051/0004-6361/202040108>
- Bullock, J. S., & Boylan-Kolchin, M. 2017, *Annual Review of Astronomy and Astrophysics*, 55, 343. <https://www.annualreviews.org/content/journals/10.1146/annurev-astro-091916-055313>
- Clowe, D., Bradač, M., Gonzalez, A. H., et al. 2006, *The Astrophysical Journal*, 648, L109. <https://dx.doi.org/10.1086/508162>
- Comerón, S., Trujillo, I., Cappellari, M., et al. 2023, *A&A*, 675, A143. <https://doi.org/10.1051/0004-6361/202346291>
- Cookson, S. A. 2024, *Monthly Notices of the Royal Astronomical Society*, 533, 110. <https://doi.org/10.1093/mnras/stae1820>
- Crovisier, J. 2011, *Oort Cloud*, ed. M. Gargaud, R. Amils, J. C. Quintanilla, H. J. J. Cleaves, W. M. Irvine, D. L. Pinti, & M. Viso (Berlin, Heidelberg: Springer Berlin Heidelberg), 1175–1175. https://doi.org/10.1007/978-3-642-11274-4_1108
- Di Cintio, A., & Lelli, F. 2015, *Monthly Notices of the Royal Astronomical Society: Letters*, 456, L127. <https://doi.org/10.1093/mnras/51/lv185>
- Dolan, B. P. 2023, *Einstein's General Theory of Relativity* (Cambridge University Press), doi:10.1017/9781009263689.004
- Frenk, C., & White, S. 2012, *Annalen der Physik*, 524, 507. <https://onlinelibrary.wiley.com/doi/abs/10.1002/andp.201200212>

- Gibbons, G. W., & Werner, M. C. 2008, *Classical and Quantum Gravity*, 25, 235009.
<https://dx.doi.org/10.1088/0264-9381/25/23/235009>
- Goddy, J. S., Stark, D. V., Masters, K. L., et al. 2023, *MNRAS*, 520, 3895.
<https://doi.org/10.1093/mnras/stad298>
- Katz, A., Reece, M., & Sajjad, A. 2016, *PDU*, 12, 24.
<https://www.sciencedirect.com/science/article/pii/S2212686416000042>
- Lelli, F., McGaugh, S. S., Schombert, J. M., Desmond, H., & Katz, H. 2019, *MNRAS*, 484, 3267.
<https://doi.org/10.1093/mnras/stz205>
- Li, Z., & Zhou, T. 2020, *Phys. Rev. D*, 101, 044043.
<https://link.aps.org/doi/10.1103/PhysRevD.101.044043>
- McGaugh, S. S. 2004, *ApJ*, 609, 652.
<https://dx.doi.org/10.1086/421338>
- McGaugh, S. S., de Blok, W. J. G., Schombert, J. M., de Naray, R. K., & Kim, J. H. 2007, *ApJ*, 659, 149.
<https://dx.doi.org/10.1086/511807>
- McGaugh, S. S., Lelli, F., & Schombert, J. M. 2016, *PhRvL*, 117, 201101. <https://link.aps.org/doi/10.1103/PhysRevLett.117.201101>
- Merritt, D. 2017, *Stud. Hist. Philos. Sci. B Stud. Hist. Philos. Modern Phys.*, 57, 41. <https://www.sciencedirect.com/science/article/pii/S1355219816301563>
- Milgrom, M. 1983, *ApJ*, 270, 365
- . 2020, *Studies in History and Philosophy of Science Part B: Studies in History and Philosophy of Modern Physics*, 71, 170. <https://www.sciencedirect.com/science/article/pii/S1355219819301972>
- Mistele, T., McGaugh, S., Lelli, F., Schombert, J., & Li, P. 2024, *The Astrophysical Journal Letters*, 969, L3.
<https://dx.doi.org/10.3847/2041-8213/ad54b0>
- Moffat, J. W., & Toth, V. T. 2009, *MNRAS*, 397, 1885.
<https://doi.org/10.1111/j.1365-2966.2009.14876.x>
- Monjo, R. 2017, *PhRvD*, 96, 103505.
<https://link.aps.org/doi/10.1103/PhysRevD.96.103505>
- . 2023, *CQGra*, 40, 235002. <https://iopscience.iop.org/article/10.1088/1361-6382/ad0422>
- . 2024, *ApJ*, 967, 66.
<https://dx.doi.org/10.3847/1538-4357/ad3df7>
- Monjo, R., & Banik, I. 2024, Anomalous radial acceleration of galaxies and clusters supports hyperconical modified gravity, , , arXiv:2405.10019
- Monjo, R., & Campoamor-Stursberg, R. 2023, *CQGra*.
<http://iopscience.iop.org/article/10.1088/1361-6382/aceacc>
- Rodríguez-Gil, P., Gänsicke, B. T., Hagen, H.-J., et al. 2005, *A&A*, 431, 269.
<https://doi.org/10.1051/0004-6361:20042026>
- Roszkowski, L., Sessolo, E. M., & Trojanowski, S. 2018, *Reports on Progress in Physics*, 81, 066201.
<https://dx.doi.org/10.1088/1361-6633/aab913>
- Sanders, R. H. 2003, *Monthly Notices of the Royal Astronomical Society*, 342, 901.
<https://doi.org/10.1046/j.1365-8711.2003.06596.x>
- Trippe, S. 2014, *Zeitschrift Naturforschung Teil A*, 69, 173
- Umetsu, K. 2020, *Astronomy and Astrophysics Review*, 28, 7. <https://link.springer.com/article/10.1007/s00159-020-00129-w>
- Will, C. M. 2014, *Living Reviews in Relativity*, 17, 4.
<https://link.springer.com/article/10.12942/lrr-2014-4>